crystals

MDPI

Article

A Probe to Surface Reactivity, Crystal Structure, and DFT Investigations for Newly Synthesized 4,5-bis(4-Nitrophenyl)-8a-phenyl-decahydro-[1,3]diazino [4,5-d]pyrimidine-2,7-dione: A Combined Theoretical and Experimental Study

Youness El Bakri [1,*], Malahat Kurbanova [2,*], Atazaz Ahsin [3], Nacaf Ramazanzade [2] and Rashad Al-Salahi [4]

[1] Department of Theoretical and Applied Chemistry, South Ural State University, Lenin Prospect 76, Chelyabinsk 454080, Russia
[2] Organic Chemistry Department, Baku State University, Z. Khalilov 23, Baku AZ 1148, Azerbaijan; necef.ramazanzade17@gmail.com
[3] Beijing National Laboratory for Molecular Sciences, Institute of Chemistry, Chinese Academy of Sciences, Beijing 100190, China; atazazahsin99@gmail.com
[4] Department of Pharmaceutical Chemistry, College of Pharmacy, King Saud University, Riyadh 11451, Saudi Arabia; ralsalahi@ksu.edu.sa
* Correspondence: yns.elbakri@gmail.com (Y.E.B.); mkurbanova72@mail.ru (M.K.)

Abstract: The multicomponent reaction of 4-nitrobenzaldehyde with acetophenone and urea in the presence of HCl was investigated, and, as a result, 4,5-bis(4-nitrophenyl)-8a-phenyl-decahydro-[1,3]diazino[4,5-d]pyrimidine-2,7-dione was synthesized. The structure of the synthesized compound was confirmed by the X-ray method. We performed Hirshfeld surfaces (HS) analysis and two-dimensional (2D) fingerprint plots for the studied compound to obtain surface reactivity and intermolecular interactions. The H···H interactions were found to be higher, up to 32.2%, while the percentage C···O contact was found to be the lowest among the reported interactions for single crystal packing. The energy framework analysis shows the strength of interaction energy within fragments of a single crystal at 3.08 A distances. The DFT study shows structural reactivity and a reduced HOMO-LUMO gap up to 4.0 eV. The NPA study reveals the reactivity and excellent charge transfer within the structure. The TD-DFT study reveals the absorbance in the UV region and excited state parameters during crucial transitions (transitions with maximum oscillator strength). The investigated compound shows excellent optical and nonlinear optical (NLO) properties, as indicated by its polarizability (αo) and hyperpolarizability (βo) values.

Keywords: multicomponent reaction; X-ray analysis; Hirshfeld surface; DFT; NLO

Citation: El Bakri, Y.; Kurbanova, M.; Ahsin, A.; Ramazanzade, N.; Al-Salahi, R. A Probe to Surface Reactivity, Crystal Structure, and DFT Investigations for Newly Synthesized 4,5-bis(4-Nitrophenyl)-8a-phenyl-decahydro-[1,3]diazino [4,5-d]pyrimidine-2,7-dione: A Combined Theoretical and Experimental Study. *Crystals* **2023**, *13*, 942. https://doi.org/10.3390/cryst13060942

Academic Editor: Sergio Brutti

Received: 19 May 2023
Revised: 2 June 2023
Accepted: 7 June 2023
Published: 11 June 2023

1. Introduction

Multicomponent reactions are obtained by producing structural complexities in one step from three or more reactants, making it feasible to synthesize target compounds with higher proficiency. Recently, the focus on multicomponent reactions has expanded in the academic literature. The revival in this area was motivated by the pharmaceutical industry. In particular, there is a need to collect libraries of structurally complex compounds to be evaluated as forefront compounds in drug discovery programs. However, the use of multicomponent reactions to achieve that substantial objective is limited considering the insufficient number of such reactions. As it is known, 3,4-dihydropyridine-2 (1H)-one(thiones) is synthesized from the multicomponent, one-step condensation of aromatic aldehydes with urea and methylene active compounds, which are highly applicable in medicine in the presence of different catalysts based on the Biginelli reaction [1–4]. The Biginelli reaction contains the three-component condensation of aromatic aldehydes, ureas,

and carbonyl compounds, which allows the preparation of hydrogenated pyrimidine-2 among compounds with high biological activity. Thus, research on the modification of the Biginelli reaction using aromatic ketones is crucial [5,6]. As a consequence of the Biginelli synthesis, heterocyclic systems of dihydropyrimidinones are established, which are significant in the construction of biomolecules, including DNA and RNA. The Biginelli reaction ensures wide product diversity with the inclusion of various pharmacophoric groups in the structure of dihydropyrimidines, which provide favorable supramolecular interactions with a specific biological target and trigger or block its biological response, considering the multicomponent nature of this reaction. Biological structures developed by living organisms have their chemical roots in molecular (covalent) and supramolecular (non-covalent) morphogenesis. Hence, they are at the frontiers of physics, chemistry, biology, and other disciplines of the life sciences. Unfortunately, not all supramolecular nucleators are biodegradable, bioabsorbable, or nontoxic. The potential problems with some of those organic compounds can be a significant concern in the biomedical field. Thus, polylactide matrices have also been blended with harmless biobased nucleating agents (e.g., orotic acid, humic acids, fulvic acids, nanocellulose, and cyclodextrins). As mentioned above, heterocyclic compounds have a broad range of applications, including medicinal chemistry, agrochemicals, polymers, and products from various industries. To be more precise, nitrogen-containing heterocycles are very common in nature and can be found in many natural products such as alkaloids, vitamins, antibiotics, and hormones. The pyrimidine nucleus is a necessary class of heterocyclic compounds for their medicinal properties due to the presence of pyrimidine bases in uracil, cytosine, and thymine, which form the building blocks of DNA and RNA. As pyrazolopyrimidines have structural similarities with purines, they are considered biologically active isomeric purine analogs present in DNA and RNA. Pyrazolo[3,4-d]pyrimidines are reported to have different pharmacological properties as antiviral, anticoagulant, antimicrobial, antitumor, analgesic, and antileukemic agent. Recently, the pyrazolo[3,4-d]pyrimidine ring system has been a significant phar-macophore for anticancer drug discovery. Pyrazolo[3,4-d]pyr-imidines are potent and selective inhibitors of many kinases, which have a key role in cancer cell proliferation [7–10].

2. Materials and Method

2.1. Chemicals

Synthesis of 4,5-bis(4-nitrophenyl)-8a-phenyl-decahydro-[1,3]diazino[4,5-d]pyrimidine-2,7-dione (**I**).

To a solution of 9.0 g (150 mmol) of urea in 70 mL of ethanol and 5 mL of HCI, 50 mmol of the corresponding 4-nitroaldehyde was added. The reaction was mixed and left at room temperature overnight. Then, 6.0 g (50 mmol) of acetophenone was added to the reaction mixture, and boiled for 3 h, and another 3.0 g (50 mmol) of urea was added and kept to boil for 3 h. After cooling, the sediment was filtered off, washed successively with water and ethanol, dried and 4,5-bis(4-nitrophenyl)-8a-phenyl-decahydro-[1,3]diazino[4,5-d]pyrimidine-2,7-dione (**I**) was obtained in 75% yield. The improvement in the reactions as well as the clarity of the synthesized compounds was traced by thin-layer chromatography (TLC). X-ray diffraction data confirmed the structure of compound (**I**). Yield, 75%, mp = 325–330 °C.

2.2. X-ray Analysis

A single crystal of 4,5-bis(4-nitrophenyl)-8a-phenyl-decahydro-[1,3]diazino[4,5-d] pyrimidine-2,7-dione (**I**) suitable for X-ray analysis (Figure 1) was obtained by twofold recrystallization from ethanol. Crystallographic data and the parameters of the X-ray diffraction experiments are presented in Tables 1 and 2. The whole set of X-ray diffraction data for compound (**I**) was deposited to the Cambridge Crystallographic Data Centre (CCDC entry no. 2246331) and is available at www.ccdc.cam.ac.uk (accessed on 6 March 2023).

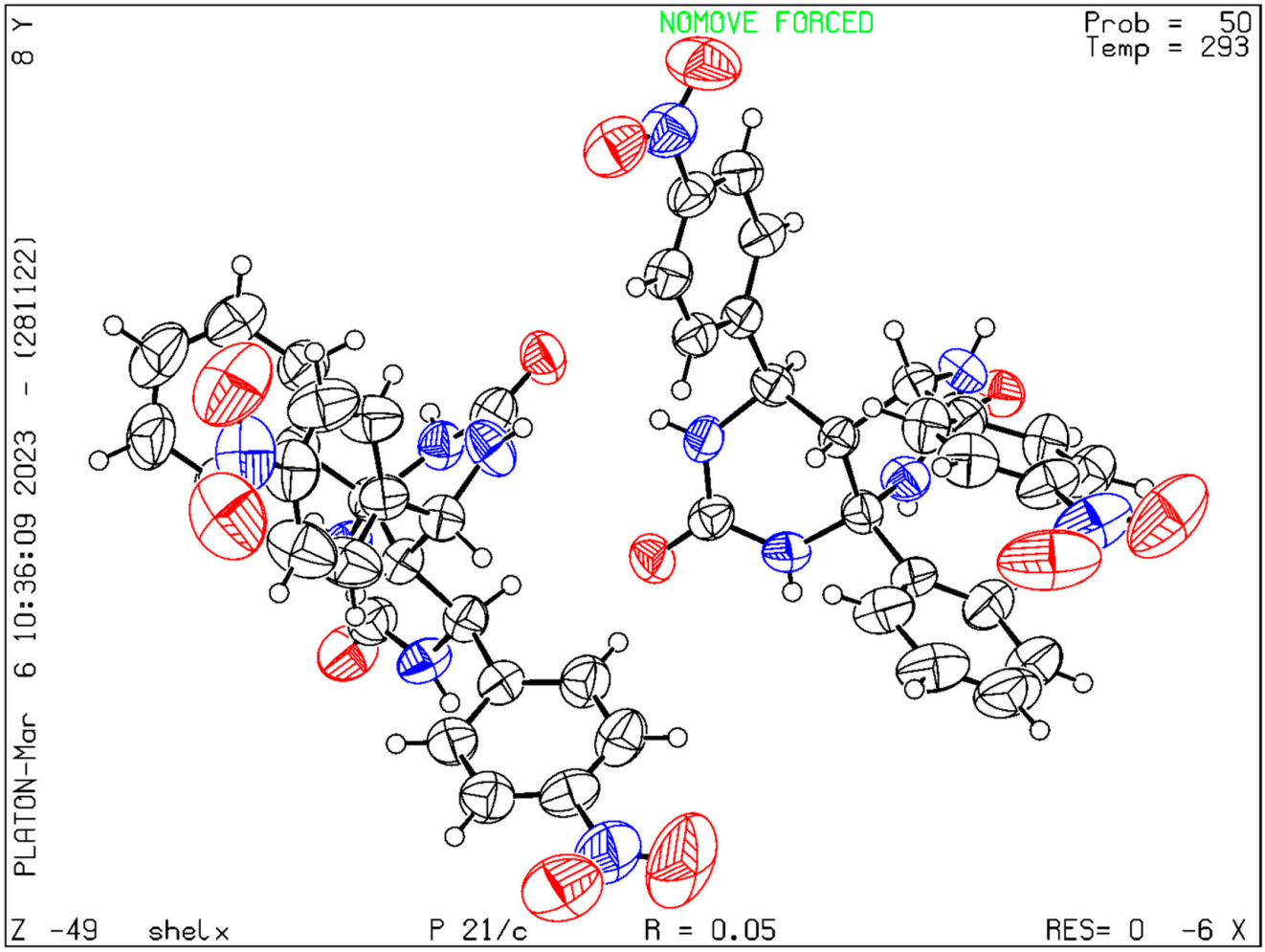

Figure 1. Structure of the molecule of **I** according to the X-ray diffraction data (blue = N atom; red = O atom).

2.3. Hirshfeld Surface Analysis

Crystal Explorer 21.5 software was used to perform Hirshfeld surfaces (HS) analysis and two-dimensional (2D) fingerprint plots [11]. This analysis is a valuable theoretical tool for visualizing and analyzing intermolecular interactions between the molecular pairs of crystals. The use of Hirshfeld surfaces in combination with fingerprint (FP) plots demonstrated the weak interactions that are important for the packing of crystals and the reactivity of crystals [12].

2.4. DFT Study

Density functional theory (DFT) is known to be the most viable method for investigating the electronic and optical properties of molecules and compounds. The FMO, NBO, and global reactivity descriptors are extensively used quantum chemical tools to sketch the reactivity and stability of newly synthesized organic compounds. In the DFT study, we mainly adopted B3LYP (hybrid) functional for electronic and optical properties.

All chemical simulations were performed in the gas phase to understand the reactivity and optical properties of the compound [13]. The hybrid DFT functional B3LYP in combination with the 6-31+G(d,p) basis set is previously reported for similar organic compounds [14]. Furthermore, the choice of this method is consistent with previously reported studies on photochromic and supramolecular compounds. The Gaussian 09 program package was used for all the simulations [15]. The GaussView 09 software was employed to draw molecular structures and for the visualization of optimized geometries.

After optimization, the frequency calculation was performed to confirm the stability of molecular geometry. Frontier molecular orbital (FMO) and NBO charges were calculated to obtain the reactivity and stability of the studied compound. Furthermore, global reactivity descriptors, including ionization potential (IP), electron affinity (EA), chemical hardness (η), chemical potential (μ), electronegativity (χ), and electrophilicity index (ω), were also calculated. Density of states (DOS) analysis was performed to gain further insight into the electronic and conductivity of the studied compound. The DOS spectrum is plotted by using GaussSum 3.0 software. A molecular electrostatic potential (MESP) study was performed to visualize the reactivity and electron-rich site of the compound.

Table 1. Basic crystallographic data and refinement parameters for compounds (**I**).

Parameters	Value
	I
Empirical formula	$C_{24}H_{20}N_6O_6$
M	488.46
Temperature, K	293
Crystal size, mm^3	0.19 × 0.18 × 0.16
Crystal system	Monoclinic
Space group	$P2_1/c$
a, Å	12.6302 (10)
b, Å	12.5115 (13)
c, Å	29.265 (2)
β, deg	100.174 (6)
V, $Å^3$	4551.8 (7)
Z	8
ρ_{calcd}, g/cm^3	1.426
μ, mm^{-1}	0.11
F (000)	2032
Nref	7076
h, k, l_{max}	14, 14, 33
S	0.818
Npar	681
Data completeness	0.993
R (reflections)	0.0465 (2455)
wR2 (reflections)	0.0924 (7076)
Theta (max)	23.968
Δρmax, Δρmin (e $Å^{-3}$)	0.16, −0.16

Table 2. Hydrogen bond geometry (Å, °).

D—H···A	D—H	H···A	D···A	D—H···A
C33—H33···O5	0.98	2.51	3.423 (5)	156
C2—H2···O10 [i]	0.93	2.56	3.480 (6)	173
C31—H31···O7 [ii]	0.98	2.38	3.121 (6)	132
C23—H23···O1 [iii]	0.93	2.63	3.401 (6)	140
N6—H6···O6 [iv]	0.78 (3)	2.11 (3)	2.893 (5)	178 (3)
N3—H3···O11	0.79 (3)	2.17 (3)	2.940 (5)	162 (3)
N5—H5···O5 [v]	0.77 (3)	2.30 (3)	2.998 (5)	151 (3)
N12—H12*A*···O6 [v]	0.83 (3)	2.15 (3)	2.961 (5)	169 (3)
N10—H10···O11 [vi]	0.84 (4)	2.03 (4)	2.870 (5)	178 (4)

Symmetry codes: (i) $-x+1, y+1/2, -z+3/2$; (ii) $-x+1, y-1/2, -z+3/2$; (iii) $-x+2, y-1/2, -z+3/2$; (iv) $-x+2, -y, -z+1$; (v) $-x+1, -y, -z+1$; (vi) $-x+1, -y+1, -z+1$.

Moreover, the optical and nonlinear optical (NLO) properties of the studied compound were determined by dipole moment (μ_o), polarizability (α_o), hyperpolarizability (β_o), and vector part of hyperpolarizability (β_{vec}) at the same function.

3. Results and Discussion

3.1. Chemical Synthesis

As is known, multicomponent reactions have become a constantly developing method for obtaining new biologically active compounds and drugs. They generate, with the contribution of three or more compounds, a new product that consists of the primary structural parts of all the original molecules. Given the above, we set out to continue research on the modification of the Biginelli reaction using aromatic ketones. Acetophenone was chosen as the aromatic ketone for the study. Condensation of benzaldehyde, acetophenone, and carbamide in ethanol in the presence of concentrated HCl led to the formation of compound (**I**) (Schemes 1 and 2).

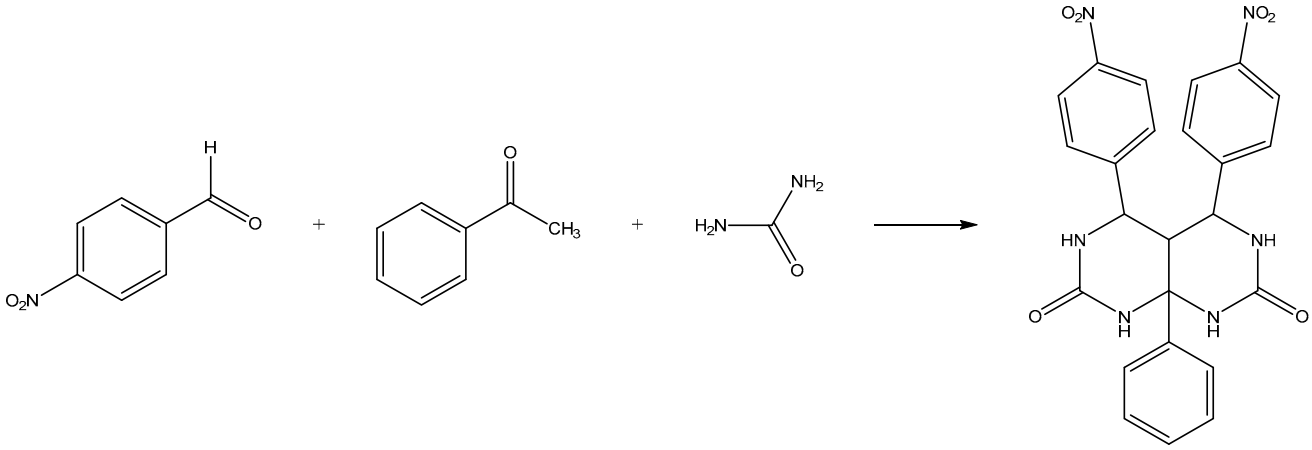

Scheme 1. Synthesis of 4,5-bis(4-nitrophenyl)-8a-phenyl-decahydro-[1,3]diazino[4,5-d]pyrimidine-2,7-dione (**I**).

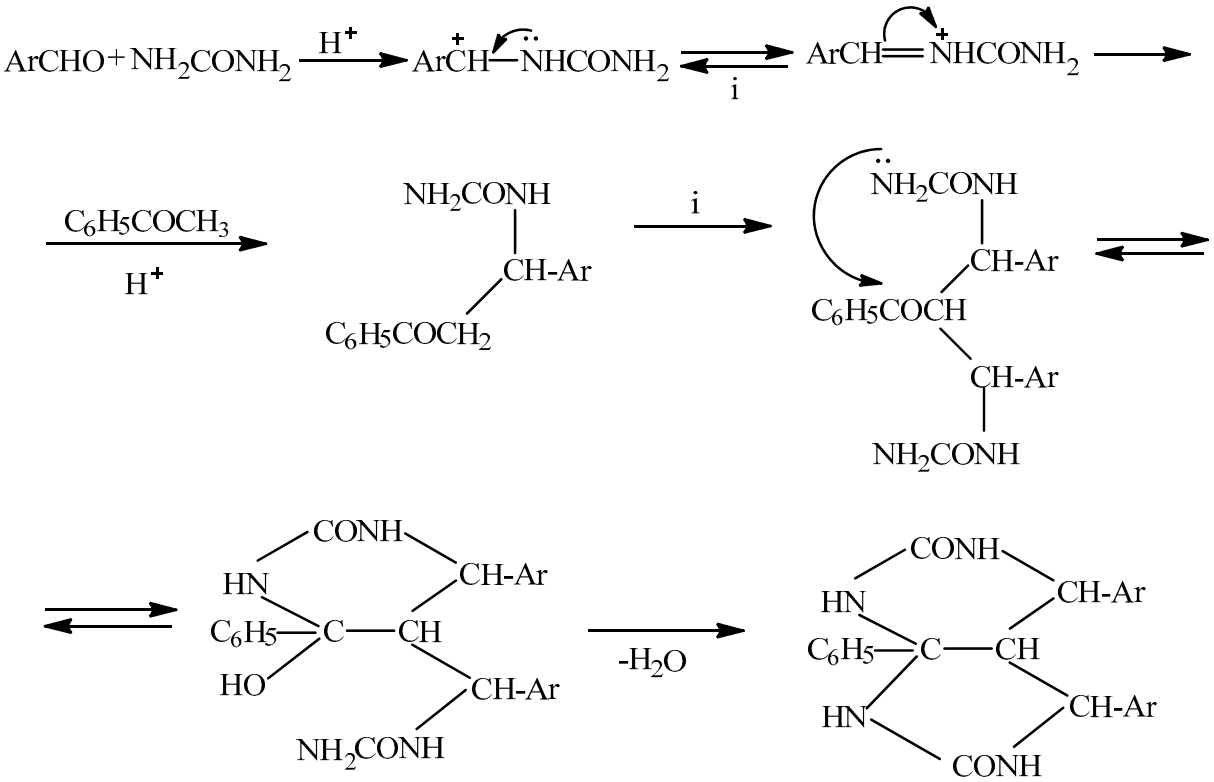

Scheme 2. Mechanism synthesis of compound (**I**).

3.2. Hirshfeld Surfaces (HS) Analysis

In terms of crystal packing, the various non-covalent interactions are the most important to investigate because they provide us with unique information about the arrangement of molecules throughout the crystalline material. Points where the electron density contribution from the molecule of interest is equal to the contribution from all other molecules define the Hirshfeld surface encompassing the molecule. There are two distances defined for any given location on the isosurface: de, the distance to the nearest external nucleus, and di, the distance to the nearest internal nucleus. The 3D HS surface plots of d_{norm}, di, de, and the shape index are given in Figure 2. In d_{norm}, three different colors (red, blue, and white) show a range of non-covalent interactions with neighbor fragments. Graphical plots of the molecular Hirshfeld surfaces were mapped with d_{norm} using a red–white–blue color scheme, where red highlights shorter contacts, white is used for contacts around the wander walls radii separation, and blue is for longer contacts. The red color on the HS surface indicates that the space among the atoms is smaller or equal to the summation of van der Waals radii of the involved atoms. For the given d_{norm} surface, the presence of a red spot indicates strong intermolecular interactions with neighbor fragments. The red color spots appeared around the nitro group of the compound and another spot near the CH of the benzene ring. On the other hand, the white spots and blue regions indicate relatively weak interactions and negligible interactions, respectively. The values of d_{norm}, di, de, and the shape index are given in Table 3. The minimum values of di and de were 0.75 Å, while the maximum values increased to 2.98 Å and 2.83 Å, respectively. A surface's curvedness can be thought of as a quantitative measure of its "how many shapes"; a low value of curvedness corresponds to relatively flat regions, while a high value of curvedness is characteristic of regions with sharp curvature and tends to divide the surface into patches that are associated with contacts between neighboring molecules. The shape index is a measure of "which shape", and it is especially sensitive to localized changes in surface shape, especially in regions with low total curvature (or curvedness).

Table 3. Hirshfeld surface (HS) analysis (de and di are in Å).

	Compound ($C_{24}H_{20}N_6O_6$)		
	Minimum	**Mean**	**Maximum**
di (Å)	0.7564	1.7575	2.9874
de (Å)	0.7593	1.7764	2.8371
d_{norm}	−0.5783	0.5396	1.4363
Shape index	−0.9957	0.2180	0.9990
curvedness	−4.2126	−1.0243	0.2362

The volume of the studied crystal is v = 573.09 $Å^3$, while its area is a = 450.74 $Å^2$. Additionally, the Hirshfeld surface (HS) provided information about the global shape, i.e., asphericity (Ω) and globularity (G). The anisotropy of a molecule can be quantified by its asphericity (Ω), which takes on the values 0 and 1 for isotropic and prolate objects, respectively. The obtained asphericity (Ω) value is 0.08, which is nearly zero and indicates the near isotropic nature, while a globularity (G) value (0.740) less than unity indicates the deviation from the spherical surface of the studied crystal.

Finding the contribution of interatomic contacts within crystal to the stabilization of the crystal packing can be adopted to quantitatively express the non-covalent interactions. For understanding the elemental interactions and their contribution to stabilizing a crystal, we plotted 2D fingerprint spectra, which are given in Figure 3. The combination of d_i (internal) and d_e (external) in the form of a 2D fingerprint plot provides a summary of intermolecular interactions in the crystal. For the studied crystal, the dominant interactions were obtained by hydrogens (H···H), which are up to 32.2%, followed by 20% of O···H interactions. These interactions are from the inside atoms (di) to outside atoms (de), and the blue color represents the contact zone of each element of different fragments within

the crystal. The least inside (di) to outside (de) interaction is found for O···C (2.6%) of the studied crystal.

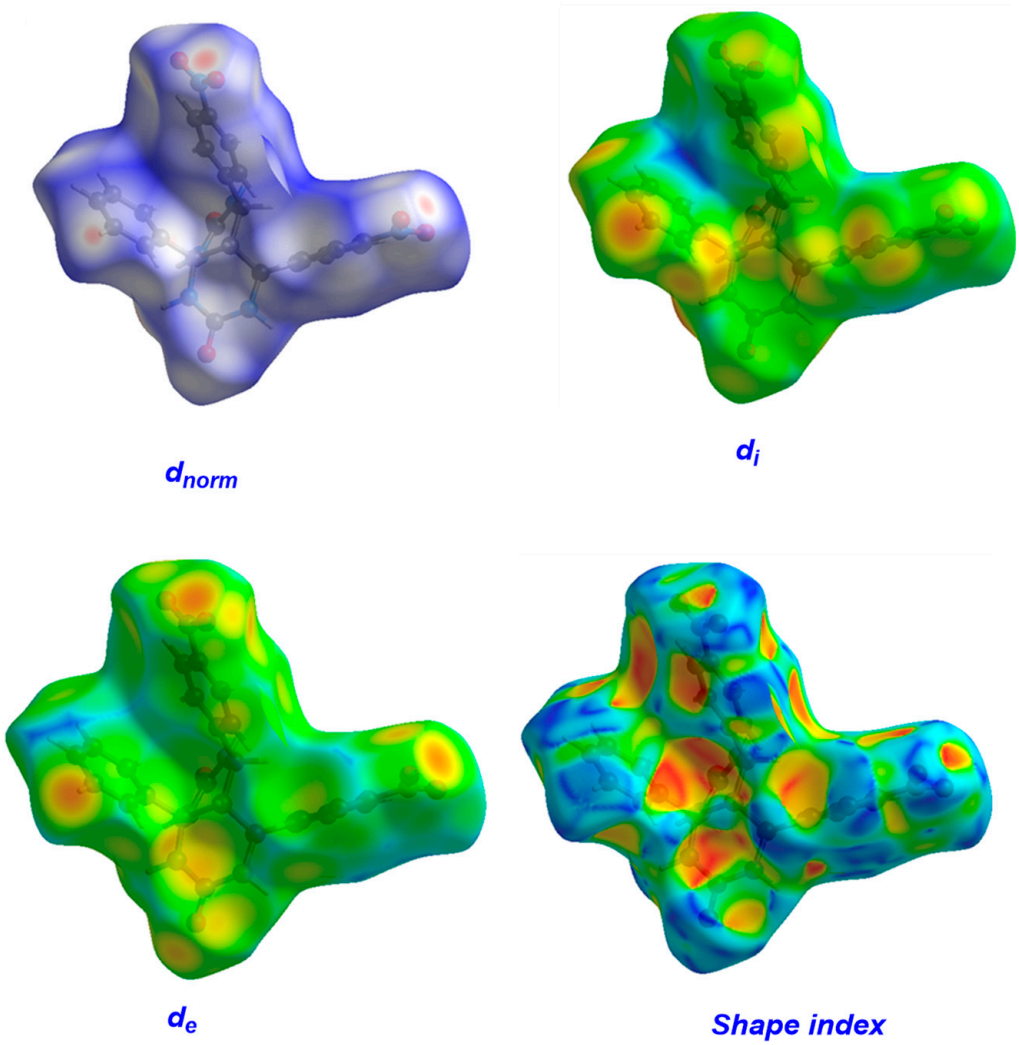

Figure 2. 3D Hirshfeld map of compounds.

3.3. Energy Framework Analysis

The energy framework analysis for the crystal packing of the studied compound is carried out using CrystalExplorer17 at B3LYP/6-31G(d,p) functional with the scale factors of k_disp = 0.871, k_ele = 1.057, k pol = 0.74 and k rep = 0.618. The different forces involved in the packing of the compound were calculated by generating a cluster of molecules within the radii of 3.08 Å around the selected central fragments molecule. The results obtained are tabulated in Table 4, which summarizes the different forces, such as electrostatic (E_{ele}), dispersion (E_{disp}), polarization (E_{pol}), repulsion energies (E_{rep}), and total energy (E_{total}). The overall energy of the studied compound is −387.8 kJ/mol. The 3D presentation of the energy framework analysis of the studied compound is shown in Figure 4. For the energy framework, we have used an energy cut-off of 20 eV to construct the coulomb energy, dispersion energy, total energy, and total energy annotated. The thickness of the cylinder connecting different fragments indicates the strength of interaction forces in packing a crystal. It is found that the electrostatic energy contribution is dominant among the other energies.

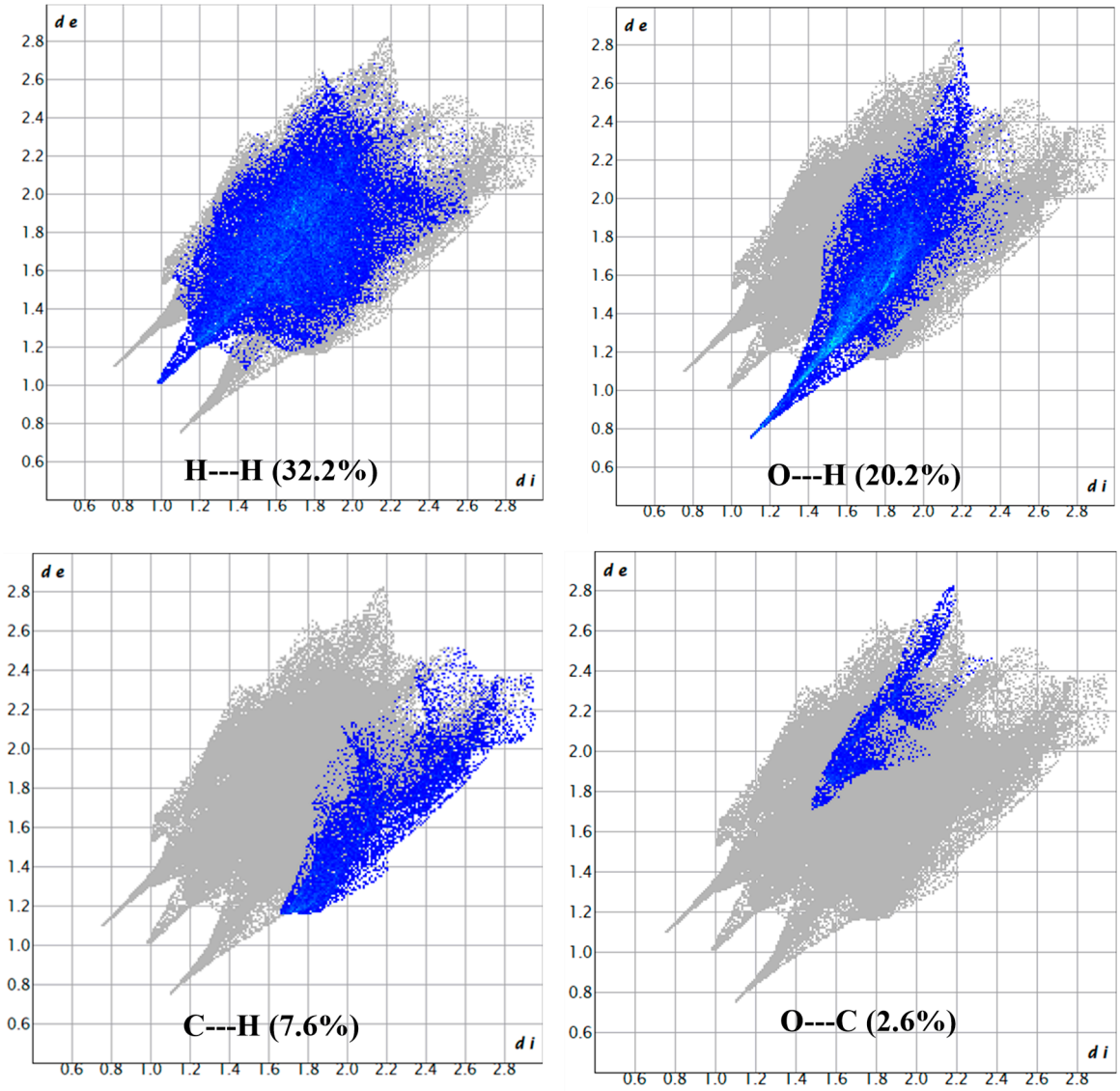

Figure 3. 2D fingerprint spectra for inside-to-outside interactions.

Table 4. Interaction Energies (kJ/mol). R is the distance between molecular centroids (mean atomic position) in Å.

N	Symop	R	E_ele	E_pol	E_dis	E_rep	E_tot
1	-	7.55	0.5	−12.0	−57.6	19.9	−43.1
0	−x, −y, −z	10.49	−21.7	−7.3	−12.9	3.7	−35.5
1	-	9.59	−8.6	−8.0	−47.5	19.7	−40.8
1	-	10.08	6.9	−2.7	−16.5	7.7	−3.3
0	-	8.09	−33.0	−9.5	−35.5	14.1	−60.3
0	-	9.57	−29.4	−13.7	−30.3	22.9	−47.6
0	-	13.32	−18.6	−2.5	−6.4	0.0	−26.3
0	x, y, z	12.51	−9.1	−2.5	−15.1	0.0	−24.6
0	-	7.98	−37.2	−21.0	−37.6	37.0	−55.5
0	−x, −y, −z	9.97	−84.8	−26.1	−24.9	61.9	−75.7
0	−x, y + 1/2, −z + 1/2	9.65	−19.4	−5.0	−27.5	10.4	−39.4
0	-	10.40	−1.9	−3.6	−26.5	8.1	−21.6
	Total energy						−387.8

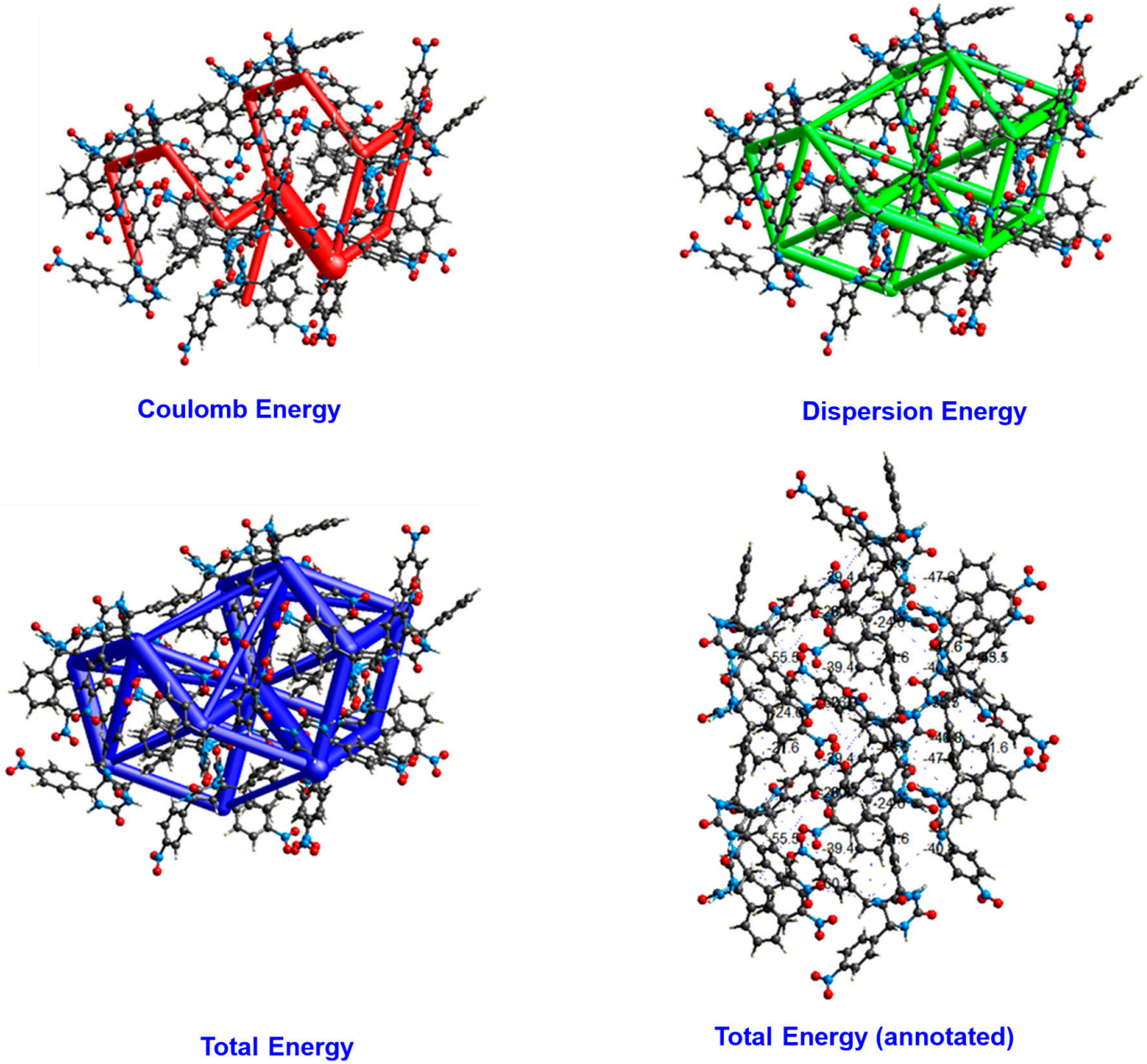

Figure 4. 3D energy framework analysis of the studied compound.

3.4. DFT Analysis

3.4.1. Optimized Geometry of Studied Compound

Initially, we obtained an optimized structure without any geometry constraints at B3LYP/6-31+G(d,p) functional. The compound has C1 point group symmetry. The optimized structure of the compound is given in Figure 5. The total energy of the compound is −1706.41 Hartree. The C–C bond length for the intact benzene rings is 1.39 Å, which is identical to that experimentally measured. An increase in bond length (1.55 Å) between C–C can be seen in a heterocyclic six-membered ring, which corresponds to a single bond. The performed frequency calculations analysis indicates that the structure is true minima on the potential energy surface and has no imaginary frequency associated with it.

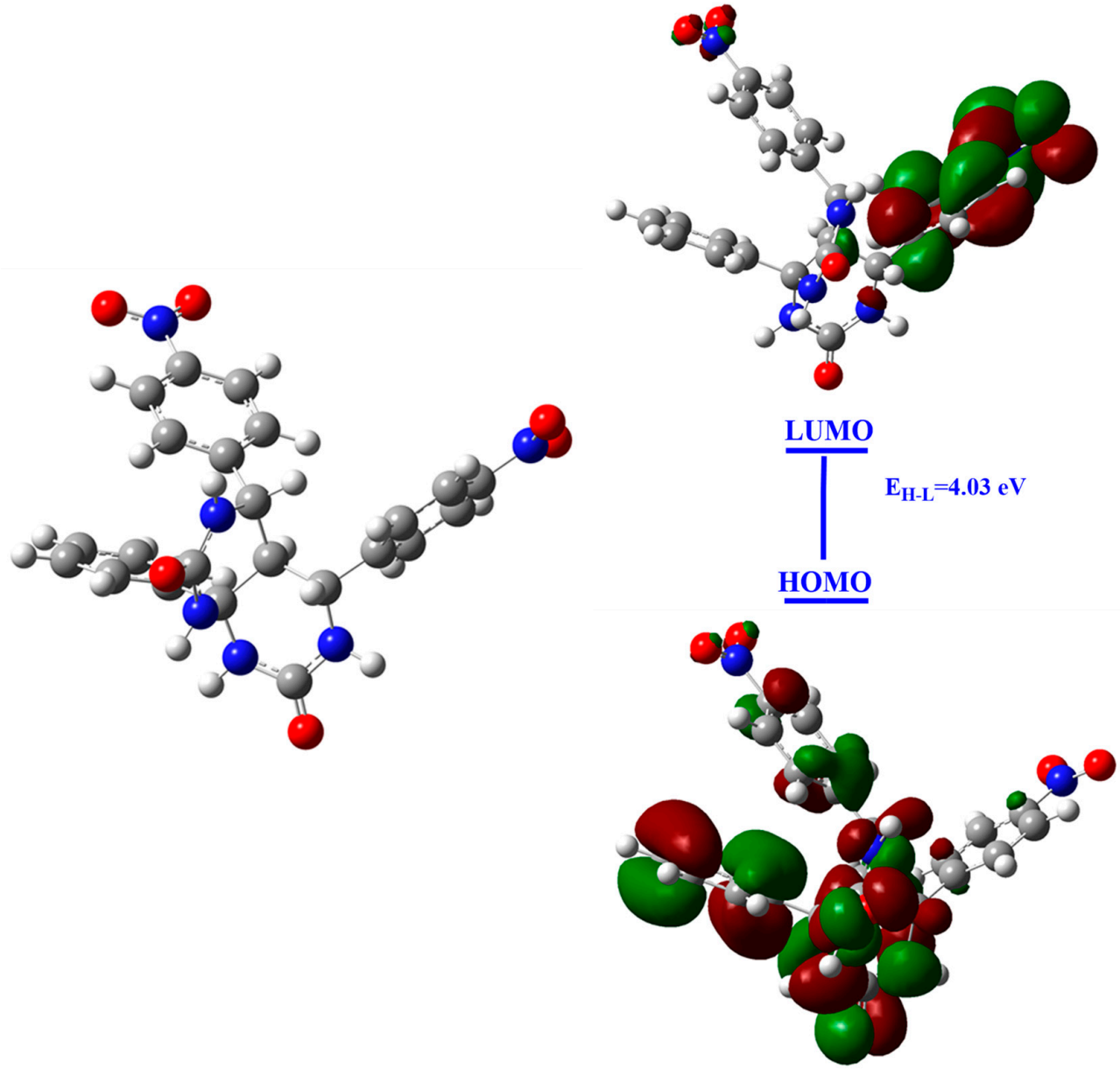

Figure 5. Optimized geometry and HOMO-LUMO plots at B3LYP/6-31+G(d,p).

3.4.2. Mulliken's Atomic Charges and FMO Analysis

The entire hydrogen atoms show positive mulliken's charges and act as electron acceptor atoms (lewis acid). All the computed mulliken charges are shown in Table 5. The atomic charges obtained on nitrogen atoms are negative and range from −0.34 to −0.69 e. The higher magnitude (negative) of nitrogen is observed for heterocyclic nitrogen, while the lowest value (−0.34) can be seen in the nitrogen of the nitro group (NO_2). Likewise, entire carbons have negative charges, except for the carbons that are attached to a nitrogen atom. Thus, the nitrogen atoms are donors, and the charge is transferred from carbon to nitrogen inside the ring.

Table 5. Mulliken's atomic charges of the studied compound.

Atoms	Charge	Atoms	Charge	Atoms	Charge
1O	−0.429510	19C	0.126098	36C	0.164288
2O	−0.439976	20H	0.141425	37O	−0.024438
3N	−0.372600	21C	0.589265	38O	0.000959
4N	−0.575703	22H	0.139331	39C	−0.033118
5N	−0.608828	23C	0.305970	40H	0.103148
6N	−0.009338	24C	−0.545560	41C	−0.363958
7O	0.116045	25H	0.091652	42H	0.101357
8C	0.138310	26C	0.140567	43C	−0.237432
9H	0.005341	27H	0.115648	44H	0.088397
10 O	0.267182	28C	−0.172610	45C	−0.412813
11C	0.356575	29H	0.114955	46H	0.066000
12C	−0.378345	30C	−0.145976	47C	0.111632
13N	0.963146	31H	0.066267	48H	0.079510
14C	0.129359	32C	0.092904	49C	−0.045811
16C	0.397683	33C	−0.367934	50H	0.085517
17C	−0.215797	34H	0.088038	51C	0.047120
18H	0.080191	35N	−0.302980	52H	0.075031
				53H	0.250129
				54H	0.220666
				55H	0.219381
				56H	0.067541

Frontier molecular orbital (FMO) analysis is a valuable theoretical tool to investigate the reactivity, kinetic stability, and optical properties of newly synthesized compounds. The FMO study includes the energy of occupied molecular orbitals (HOMO), lowest unoccupied molecular orbitals (LUMO), and their HOMO-LUMO gaps ($E_{H\text{-}L}$). Generally, the molecules with small HOMO-LUMO gaps are said to be soft in nature and have higher reactivity. This also indicates less kinetic stability and better optical properties. Compounds with narrower band gaps can be used to manufacture optoelectronic devices. The compound's HOMO energy is −7.41 eV, while its LUMO energy is 3.38 eV. The higher HOMO energy has resulted in a reduction in the HOMO-LUMO gap of about 4.03 Ev. As a result, the studied compound has small energy gaps and can be classified as a reactive organic compound.

Furthermore, we have calculated the natural population analysis (NPA) to gain deep insight into the reactivity and donor-acceptor behavior of the studied compound. The reported NPA charges on entire oxygen atoms are negative and range from −0.37 to −0.65 |e|, where the highest (negative) charge is recorded on oxygen attached to carbon (C=O). Overall, the highest value of calculated NPA charges is given in Table 6. The negative charge on nitro oxygen is smaller, which may be attributed to insufficient charge transfer compared with carbon. As carbon is more electropositive compared to nitrogen, higher charge separation is observed. Interestingly, the NBO charges on nitrogen atoms vary from positive (+0.49) to significantly negative (−0.78 |e|). Hence, the donor ability of the N-atom is more pronounced for the heterocyclic nitrogen atom compared to the nitro group. However, all carbon atoms, with the exception of those that are bonded to electronegative atoms (O, N), have negative NPA charges.

To better understand the chemical reactivity and structural features of the studied compound, we have calculated global reactivity parameters at the same level of theory. The simulated parameters include vertical ionization energy (IE), electron affinity (EA), chemical hardness (η), chemical potential (μ), electronegativity (χ), and electrophilicity index (ω); given by the following equations;

$$\text{Ionization energy (IE)} = -E(\text{HOMO})$$

$$\text{Electron affinity (EA)} = -E(\text{LUMO})$$

$$\text{Chemical Hardness } (\eta) = \frac{1}{2}\,(\text{IE} - \text{EA})$$

$$\text{Chemical potential } (\mu) = -\frac{\text{IE} + \text{EA}}{2}$$

$$\text{Electronegativity } (\chi) = -\mu$$

$$\text{Electrophilicity index } (\omega) = \frac{\mu^2}{2\eta}$$

Table 6. Point group symmetry, total electronic energy (in Hartree), negative frequency, NPA charges (O/N in |e|), the energy of HOMO (E_H in eV), the energy of LUMO (E_L in eV), HOMO-LUMO gap ($E_{H\text{-}L}$ in eV), ionization energy (IE in eV), electron affinity (EA in eV), chemical hardness (η in eV), chemical potential (μ in eV), and electronegativity (χ in eV) of the studied compound.

Point Group Symmetry	**C1**
Total electronic energy	−1706.413579
Imaginary frequency	0
Q (O/N/)	−0.65/−0.71
E_H	−7.415
E_L	−3.384
$E_{H\text{-}L}$	4.03
Ionization energy (IE)	7.45
Electron affinity (EA)	3.38
Chemical hardness (η)	2.03
Chemical potential (μ)	−5.41
Electronegativity (χ)	5.41

Ionization energy (IE) and electron affinity values are calculated by using Koopmans' theorem, where the negative of HOMO is taken as ionization potential, while the negative of LUMO is considered electron affinity (EA). The obtained value of IE for the studied compound is 7.45 eV, while its EA is 3.38 eV. The computed significant IE value indicates the electronic stability of the compound. It also suggests a less electropositive nature and the high amount of energy required to remove an electron. On the other hand, a compound is favorable for gaining extra electrons. Quantum chemical hardness is another parameter to classify the reactivity and soft nature of the compound. The obtained value of chemical hardness is 2.03 ev, and the molecule is said to be soft in nature. The higher the softness, the more the reactivity of the molecule further derives from a chemical reaction. Similarly, the calculated value of chemical potential is −5.41 eV. The calculated electronic chemical potential (μ) measures the tendency of electrons to escape from an equilibrium system. The more negative value (−5.41 eV) of chemical potential observed shows that this molecule is more stable because it will retain the electron to escape from the system.

3.4.3. MESP and DOS Analysis

For any chemical species, the molecular electrostatic potential (MEP) surface has frequently been used to produce the electrostatic potential (ESP) map using constant electron density [16]. The presence of red color around the nitro group and C=O group indicates the donor site of molecules. The red area of high electron density is an ideal location for driving an electrophilic addition reaction. The central portion of the molecule, on the other hand, is blue, indicating that it has electron-deficient sites. There are no

conjugated or electronegative atoms in the center of the molecule. As a result, nitro groups (NO_2) are more unpredictable and have an electron-drawing effect on the benzene ring. This effect removes electrons from the rest of the molecule, making it electron-deficient while being electron-rich around the nitro group.

Density of states (DOS) analysis is performed to further understand the electronic properties and reactivity of the compound. We determined the total density of state (TDOS) and the spectrum is plotted between the energy range of −21 and 5.44 Ev (Figure 6). The DOS analysis is a number of states per unit of energy, and newly generated HOMO states indicate the conductivity of the compound. The HOMO energy line appeared at −8.16 Ev, while LUMO states were near −2.72 Ev. The greater the energy of HOMO, the more electrons will be transferred to LUMO. As a result, there is a significant reduction in HOMO-LUMO gaps, and charge transfer becomes faster.

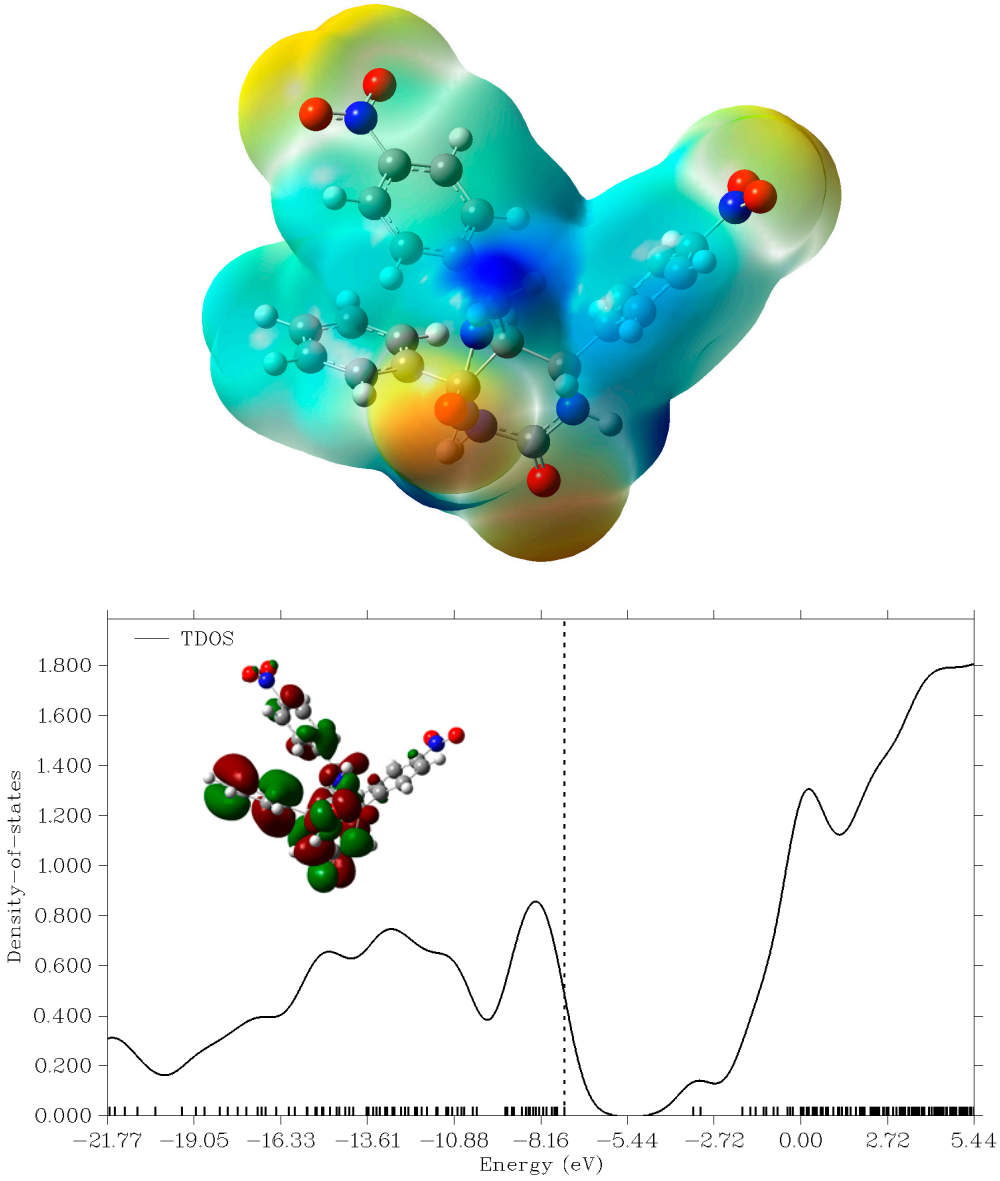

Figure 6. 3D MESP surface and DOS spectrum.

3.4.4. TD-DFT Study and Dipole Moment

We performed excited state analysis by using time-dependent density functional theory (TD-DFT) with the same method. The excited state analysis is carried out by considering 40 states (singlet and triplet) to calculate parameters, including excitation energy (ΔE) during the crucial transition, oscillator strength (f_o), and absorbance wavelength (λ). The obtained excitation energy (ΔE) value is 4.21 Ev, while its absorbance is 294.21 nm. The absorbance maxima (λ_{max}) are blue-shifted, which is indicated by a high transition energy (ΔE). These parameters are associated with a crucial transition (a transition with a maximum value of oscillator strength). We have also calculated the orbital contribution from the second crucial transition (second higher oscillator strength). The other significant percentage contribution to the electronic transition is given in Table 6. The obtained value of oscillator strength (f_o) is up to 0.046 au, where the second highest value is 0.34 au. Moreover, the orbital contribution of a particular HOMO to LUMO is given in Table 6.

The dipole moment (μ_o) is the product of charges and distances between charges. The obtained dipole moment value of the studied compound is 2.49 D. The nonzero dipole moment indicates the asymmetric charge distribution within the molecule. The measured total dipole moment is the sum of individual bond dipoles. Additionally, the polarity of molecules can be illustrated by using dipole moments. Hence, the studied compound has remarkable electronic and optical properties, which prompted us to further investigate the nonlinear optical properties of compounds.

3.4.5. Nonlinear Optical Properties of the Compound

Nonlinear optical (NLO) materials have gained popularity in the study community due to their widespread applications in data storage devices, optical switching, and laser-based endoscopy. As a result, material chemists have been interested in the hunt for new NLO compounds. Organic non-linear optical materials have several orders of magnitude and faster reaction times when compared to inorganic materials because they are made up of conjugated molecules that enable electrons to easily travel between donor and acceptor groups to facilitate charge transfer. Organic moieties with delocalized pi-electron distribution have been widely researched for possible uses in optical signal processing, optical switching, and optical power limiting, all of which require a large and fast NLO response. Because the effects are mainly caused by electronic polarization, the NLO response of many organic materials is extremely fast; thus, the NLO properties of pi-conjugated systems have received special attention.

The polarizability (α_o) of molecules is called the liner optical response, and its higher value indicates the extent of polarization in the studied molecule. In our synthesized molecule, the α_o value increased and was recorded at 342.53 au. The notable value obtained also suggests asymmetric electronic density and the presence of polarity in the molecule. Furthermore, the calculated static first hyperpolarizability (β_o) is a measure of the nonlinear optical response. The presence of conjugation and donor-acceptor groups in the molecule is a key factor in triggering the hyperpolarizability response. The β_o value increases to 2047.66 au (see Table 7). Thus, the studied molecule has a remarkable β_o value, which indicates its NLO properties. The vector part of hyperpolarizability (β_{vec}) is the measured projection of hyperpolarizability on the dipole moment vector. The β_{vec} value was recorded up to 1931.60 au and had a strong correlation with total hyperpolarizability (β_o). Hence, the studied molecule has potential electronic and NLO properties and can be used for optoelectronic applications.

Table 7. Excitation energy (ΔE in eV), maximum absorbance (λ_{max} in nm), oscillator strength (f_o in au), dipole moment (μ_o in Debye), polarizability (α_o in au), polarizability volume (α_v au), hyperpolarizability (β_o in au), and projection of hyperpolarizability (β_{vec} in au) of the studied compound.

Excitation Energy (ΔE)	**4.2141**
Absorbance wavelength (λ)	294.21 nm
Oscillator strength (f_o)	0.0466
Orbital contribution	HOMO → LUMO + 4 (23%) HOMO → LUMO + 3 (6%) HOMO → LUMO + 5 (9%) HOMO → LUMO + 2 (43%)
Dipole moment (μ_o)	2.491573
Polarizability (α_o)	342.53
Polarizability volime	50.75
Hyperpolarizability (β_o)	2047.668
(β_{vec})	1931.60

4. Conclusions

The surface reactivity and intermolecular interactions of the studied compound were investigated by Hirshfeld surface analysis. The 2D fingerprint spectra show higher elemental contact, up to 32.2% for H···H in crystal packing. Energy framework analysis shows the interaction between pairs of fragments with neighbor molecules. Furthermore, a DFT study was performed to investigate structural reactivity and stability at the B3LY/6-311+G(d,p) functional. The HOMO-LUMO gap decreased to 4.0 eV. The NPA study revealed the reactivity and excellent charge transfer within the structure. The studied molecule shows excellent optical and nonlinear optical (NLO) properties, as indicated by its polarizability (α_o) and hyperpolarizability (β_o) values. Hence, the studied compound has excellent reactivity and is a potential candidate for NLO properties. The TD-DFT study demonstrated its crucial excitation energy and absorbance in the UV region.

Author Contributions: Conceptualization, validation, data curation, writing—review and editing, Y.E.B.; methodology, writing—review and editing, visualization, supervision, M.K.; software, analysis, investigation, resources, A.A.; data curation, writing—original draft preparation, N.R.; funding acquisition, R.A.-S. All authors have read and agreed to the published version of the manuscript.

Funding: This research was funded by Researchers Supporting Project No. RSP-2023R353, King Saud University, Riyadh, Saudi Arabia.

Data Availability Statement: Data is available from the authors on request.

Acknowledgments: The authors extend their appreciation to the Researchers Supporting Project, King Saud University, Riyadh, Saudi Arabia for funding this work through grant No. RSP-2023R353.

Conflicts of Interest: The authors declare no conflict of interest.

References

1. Kaur, R.; Chaudhary, S.; Kumar, K.; Gupta, M.K.; Rawal, R.K. Recent synthetic and medicinal perspectives of dihydropyrimidinones: A review. *Eur. J. Med. Chem.* **2017**, *132*, 108–134. [CrossRef] [PubMed]
2. El Bakri, Y.; Kurbanova, M.M.; Siddique, S.A.; Ahmad, S.; Goumri-Said, S. One-pot synthesis, X-ray crystal structure, and identification of potential molecules against COVID-19 main protease through structure-guided modeling and simulation approach. *Arab. J. Chem.* **2022**, *15*, 104230. [CrossRef] [PubMed]
3. Zabihollahi, R.; Fassihi, A.; Aghasadeghi, M.R.; Memarian, H.R.; Soleimani, M.; Majidzadeh-A, K. Inhibitory effect and structure–activity relationship of some Biginelli-type pyrimidines against HSV-1. *Med. Chem. Res.* **2013**, *22*, 1270–1276. [CrossRef]
4. Kappe, C.O. Biologically active dihydropyrimidones of the Biginelli-type—A literature survey. *Eur. J. Med. Chem.* **2000**, *35*, 1043–1052. [CrossRef] [PubMed]
5. El Bakri, Y.; Kurbanova, M.; Siddique, S.A.; Karthikeyan, S.; Maharramov, A.; Ramazanzade, N. Synthesis, virtual screening, and computational approach of 6-(4-metoxyphenyl)-4-phenyl-1, 2-dihydropyrimidin-2-one as a potential target for thioredoxin glutathione reductase (TGR). *J. Mol. Struct.* **2023**, *1286*, 135623. [CrossRef]

6. Kurbanova, M.; Ashfaq, M.; Tahir, M.N.; Maharramov, A.; Dege, N.; Ramazanzade, N.; Cinar, E.B. Synthesis, Crystal Structure, Supramolecular Assembly Inspection by Hirshfeld Surface Analysis and Computational Exploration of 4-Phenyl-6-(p-Tolyl) Pyrimidin-2 (1H)-One (PPTP). *J. Struct. Chem.* **2023**, *64*, 437–449. [CrossRef]
7. Zhang, Y.; Liu, Y.; Zhou, Y.; Zhang, Q.; Han, T.; Tang, C.; Fan, W. Pyrazolo [1, 5-a] pyrimidine based Trk inhibitors: Design, synthesis, biological activity evaluation. *Bioorg. Med. Chem. Lett.* **2021**, *31*, 127712. [CrossRef] [PubMed]
8. Aydin, B.O.; Anil, D.; Demir, Y. Synthesis of N-alkylated pyrazolo [3, 4-d] pyrimidine analogs and evaluation of acetylcholinesterase and carbonic anhydrase inhibition properties. *Arch. Pharm.* **2021**, *354*, 2000330. [CrossRef] [PubMed]
9. Matos, L.H.S.; Masson, F.T.; Simeoni, L.A.; Homem-de-Mello, M. Biological activity of dihydropyrimidinone (DHPM) derivatives. *A Syst. Rev.* **2018**, *143*, 1779.
10. Khasimbi, S.; Ali, F.; Manda, K.; Sharma, A.; Chauhan, G.; Wakode, S. Dihydropyrimidinones scaffold as a promising nucleus for synthetic profile and various therapeutic targets: A Review. *Curr. Org. Synth.* **2021**, *18*, 270–293. [CrossRef] [PubMed]
11. Spackman, P.R.; Turner, M.J.; McKinnon, J.J.; Wolff, S.K.; Grimwood, D.J.; Jayatilaka, D.; Spackman, M.A. CrystalExplorer: A program for Hirshfeld surface analysis, visualization and quantitative analysis of molecular crystals. *J. Appl. Crystallogr.* **2021**, *54*, 1006–1011. [CrossRef] [PubMed]
12. Madhankumar, S.; Muthuraja, P.; Dhandapani, M. Structural characterization, quantum chemical calculations and Hirshfeld surface analysis of a new third order harmonic organic crystal: 2-Amino-4-methylpyridinium benzilate. *J. Mol. Struct.* **2020**, *1201*, 127151. [CrossRef]
13. Anju, L.S.; Aruldhas, D.; Joe, I.H.; Balachandran, S. Density functional theory, spectroscopic and hydrogen bonding analysis of fenoxycarb–water complexes. *J. Mol. Struct.* **2020**, *1201*, 127201. [CrossRef]
14. Tirado-Rives, J.; Jorgensen, W.L. Performance of B3LYP density functional methods for a large set of organic molecules. *J. Chem. Theory Comput.* **2008**, *4*, 297–306. [CrossRef] [PubMed]
15. Frisch, M.J.; Trucks, G.W.; Schlegel, H.B.; Scuseria, G.E.; Robb, M.A.; Cheeseman, J.R.; Scalmani, G.; Barone, V.; Mennucci, B.; Petersson, G.A.; et al. *Gaussian 09*; Gaussian Inc.: Wallingford, UK, 2010.
16. Arivazhagan, M.; Kumar, J.S. Molecular structure, vibrational spectral assignments, HOMO–LUMO, MESP, Mulliken analysis and thermodynamic properties of 2,6-xylenol and 2,5-dimethyl cyclohexanol based on DFT calculation. *Spectrochim. Acta Part A Mol. Biomol. Spectrosc.* **2015**, *137*, 490–502. [CrossRef] [PubMed]